CORA Cork Open Research Archive
Cartlann Taighde Oscailte Chorcaí

Title	Thermal decomposition mechanisms of hafnium and zirconium silicates at the atomic scale
Authors	Monaghan, Scott;Greer, James C.;Elliott, Simon D.
Publication date	2005-06-01
Original Citation	Monaghan, S., Greer, J. C. and Elliott, S. D. (2005) 'Thermal decomposition mechanisms of hafnium and zirconium silicates at the atomic scale', Journal of Applied Physics, 97(11), pp. 114911. doi: 10.1063/1.1926399
Type of publication	Article (peer-reviewed)
Link to publisher's version	http://aip.scitation.org/doi/abs/10.1063/1.1926399 - 10.1063/1.1926399
Rights	© 2005 American Institute of Physics, This article may be downloaded for personal use only. Any other use requires prior permission of the author and AIP Publishing. The following article appeared in Monaghan, S., Greer, J. C. and Elliott, S. D. (2005) 'Thermal decomposition mechanisms of hafnium and zirconium silicates at the atomic scale', Journal of Applied Physics, 97(11), pp. 114911 and may be found at http://aip.scitation.org/doi/abs/10.1063/1.1926399
Download date	2026-11-06 23:04:02
Item downloaded from	https://hdl.handle.net/10468/4231

UCC
University College Cork, Ireland
Coláiste na hOllscoile Corcaigh

Thermal decomposition mechanisms of hafnium and zirconium silicates at the atomic scale

S. Monaghan, J. C. Greer, and S. D. Elliott

Citation: Journal of Applied Physics **97**, 114911 (2005); doi: 10.1063/1.1926399
View online: http://dx.doi.org/10.1063/1.1926399
View Table of Contents: http://aip.scitation.org/toc/jap/97/11
Published by the American Institute of Physics



HTML ABSTRACT + LINKS

Thermal decomposition mechanisms of hafnium and zirconium silicates at the atomic scale

S. Monaghan, J. C. Greer, and S. D. Elliott[a)]
Tyndall National Institute, Lee Maltings, Cork, Ireland

(Received 16 February 2005; accepted 5 April 2005; published online 1 June 2005)

The hafnium and zirconium silicates, $(MO_2)_x(SiO_2)_{1-x}$, with $M=Hf/Zr$, are being considered as high-k gate dielectrics for field-effect transistors as a compromise between high permittivity and thermal stability during processing. Using atomic-scale models of silicates derived from hafnon/zircon, stability before and after simulated thermal annealing is calculated within a density-functional approach. These silicates are found to be thermodynamically unstable with respect to decomposition into SiO_2 and MO_2 ($M=Hf/Zr$). Segregation mechanisms on the atomic scale are studied leading to an insight as to an why SiO_2-rich mixtures undergo spinodal decomposition and why, by contrast, MO_2-rich phases are metastable, decomposing below typical process temperatures. © *2005 American Institute of Physics*. [DOI: 10.1063/1.1926399]

I. INTRODUCTION

High-k oxides are being investigated as gate dielectrics for future generation metal-oxide-semiconductor (MOS) technologies[1] and have been investigated for various material compositions and deposition conditions. High atomic number elements such as hafnium and zirconium are considered to be useful for incorporation into insulator oxides or silicates due to the resulting increase in the dielectric constant (k), and because they are believed to minimize dangling bonds at the silicon interface, thus assisting in lowering defect densities during processing.[2] Amorphous hafnia (HfO_2) and zirconia (ZrO_2) remain leading candidates as gate dielectric replacements, although their integration into the MOS gate stack poses substantial technological challenges.[2,3] One of these challenges is to ensure their stability as a single amorphous phase throughout MOS thermal processing (with temperatures ranging up to ~1000 °C). The glass transition temperatures of hafnia and zirconia are low [$T_g(HfO_2)$ ~500 °C, $T_g(ZrO_2)$ ~425 °C (Refs. 4 and 5)], but can be raised by the addition of silica [SiO_2, T_g ~1200 °C (Ref. 6)] to give amorphous silicates, albeit at the penalty of lowering the dielectric constant.

The hafnium and zirconium silicates (HSOs and ZSOs, respectively, or MSOs when referred to collectively) are mixtures with the composition $(MO_2)_x(SiO_2)_{1-x}$, with $M=Hf/Zr$. However, little is known about the structure or stability of these metal silicates, thus prompting the present computational study. Hafnon ($HfSiO_4$) and zircon ($ZrSiO_4$) are the MSOs with composition $x=0.5$. They occur naturally as minerals and are of use in geochronology and as optical waveguides; they also serve as natural hosts for the radioactive elements uranium and thorium in the Earth's crust, thus finding application for the storage of nuclear waste.[7] They are known to be thermodynamically stable up to ~1750 °C (Ref. 8) and ~1675 °C, (Ref. 9) respectively—adequate for the ca. 1000 °C anneals occurring during MOS processing. However, the thermal stability of other MSO compositions is less well understood.

There is now substantial experimental data on the annealing temperatures required to cause MSOs to crystallize. Initial work on the SiO_2-rich MSOs ($x<0.5$) found them to remain amorphous up to high temperatures.[2,10] In a study of MSOs with $x\leqslant 0.25$ deposited from chemical solution, MO_2 crystallization and phase separation are observed at 1000 °C, and the SiO_2 network is observed to remain amorphous.[5] X-ray studies of chemical-vapor-deposited 4–10-nm HSO films with $x\sim 0.4$ show no crystallization until ca. 1000 °C (Refs. 11 and 12) or 1100 °C,[13] but transmission electron microscopy (TEM) reveals some phase segregration. Experiments on ZSOs with $x\leqslant 0.5$ using remote plasma-enhanced chemical-vapor deposition on a Si substrate result in a lower $T_g(ZSO)=800-900$ °C, and phase separation into tetragonal ZrO_2 and amorphous SiO_2.[14] Amorphous ZSOs with $x=0.2$ decomposed into crystalline ZrO_2 at 900 °C.[15] Repeating these experiments on HfO_2-rich HSOs ($x\geqslant 0.5$), hafnia crystallites appear at 800 °C with $x=0.8$,[12] or at 850 °C with $x=0.6$.[11,13] Another study finds that MO_2-rich MSOs show crystallization and phase separation at 800 °C into tetragonal MO_2 and amorphous SiO_2.[5] Some of these data are summaried in Ref. 4. One consequence of phase separation is that the deleterious diffusion of dopants (B, P, and As) through HSOs is higher than that through SiO_2.[16]

These findings demonstrate that MSOs do not possess the requisite thermal stability for use as a single-phase MOS gate dielectric. Some studies have provided a deeper understanding of the decomposition process. It was concluded that phase separation is spontaneous for ZSOs in the range $0.03<x<0.16$ at 900 °C.[17] At 800 °C, amorphous SiO_2-rich MSOs are observed to separate before crystallization.[12] Based on the features of the known ZrO_2-SiO_2 phase diagram, Kim and McIntyre postulate a metastable miscibility gap for MSOs,[18] which results in two qualitatively different modes of decomposition: nucleation/growth and spinodal decomposition.[19] If there are kinetic barriers to decomposi-

[a)]Electronic mail: simon.elliott@tyndall.ie

 © 2005 American Institute of Physics

tion, segregation into MO_2+SiO_2 occurs above T_g by nucleation and growth. In spinodal decomposition the mixture is unstable (not metastable) and compositional fluctuations lead to spontaneous demixing within the amorphous phase at all temperatures. From the phase diagram derived from known experimental data, spinodal decomposition is predicted for ZSOs $0.1<x<0.6$ at typical MOS processing temperatures,[11] with nucleation and growth dominating otherwise. Evidence for these two distinct mechanisms at $x=0.4$ and $x=0.8$ has been obtained by examining the segregated microstructures using grazing-incidence x-ray scattering.[12]

An explanation of the decomposition processes must ultimately consider the atomic processes that lead to these different mechanisms. Fourier transform infrared (FTIR) has yielded most of the atomic-scale data on Hf/Zr silicates to date. For instance, the breaking of Si–O–Zr chains on thermal treatment is observed in FTIR, along with the growth of the Si–O–Si and Zr–O–Zr signals indicative of SiO_2 and ZrO_2.[14] Another FTIR study reports adsorptions in HSOs associated with Si–O–Hf bonding, even at relatively low metal concentrations.[5] In contrast, the same study on the equivalent ZSOs found reduced Si–O–Zr absorptions and an increase in those associated with symmetric Si–O–Si.

The need for further investigation of these mechanisms is clear. In fact, there is a general lack of published work on atomic-scale mechanisms underlying the decomposition of inorganic materials and our computational study is an investigation of transition-metal pseudobinary silicates. A recent first-principles study of ZSOs in the range $x<0.5$ concentrated on structural changes at low x and assumed the ZSOs to be thermodynamically stable.[20] Another work used first principles to model ZSO with $x=0.25$ (as well as $x=0.15$ with empirical potentials) and found the dielectric constant by assigning a polarizability to each Zr/Si polyhedron.[21] By contrast, our aim is to identify the driving forces behind phase segregation. Hence the focus here is on the early stage of decomposition where segregation can be explored by following atomic arrangements on the scale of a few nanometers. To this end, we develop a model for MSO mixtures with various compositions (Sec. II), and examine the energetic changes due to chemical substitution relative to the stable hafnon and zircon structures, both before and after molecular-dynamics (MD)-simulated annealing (Sec. III). It is found that decomposition of the SiO_2-rich MSOs is spontaneous and driven by bond formation typical of silica. Thermal treatment (MD simulation) enhances diffusion and silica growth, and causes atomic rearrangement in MO_2-rich regions that may be described as a precursor to the crystalline MO_2. It is also found that the MO_2-rich MSOs are metastable at $T<T_g(MO_2)$, but at higher temperatures nucleation of crystallites is observed with metal-metal distances characteristic of the monoclinic phase of hafnia and zirconia. Implications of our findings for technology applications are discussed in Sec. IV and conclusions are presented in Sec. V.

II. SIMULATION METHODS

A. Computational procedures

Structures for bulk MSOs are computed within the framework of density-functional theory (DFT) using the Vienna *ab initio* simulation program (VASP).[22] The gradient-corrected PW91 functional[23] has been applied to provide accurate geometries and reliable estimates for relative stabilities. Three-dimensional periodicity is imposed, with ultrasoft pseudopotentials,[24] and a plane-wave basis set (395-eV cutoff). A $2\times2\times2$ k-point grid is used, which converges total energies to within ±0.05 eV/cell. The convergence of self-consistent steps is accurate to 10^{-4} eV/cell. The optimization of cell parameters and atomic positions is accurate to $<10^{-3}$ eV Å^{-1}, and the estimated accuracy for ΔE_{mix} is 1 meV/cell.

DFT is now well established as an accurate and efficient parameter-free way to compute the properties of crystalline materials, similar computations having been validated on zircon[20,25] and silicates of Mg.[26] By calculating the most stable forms of the MSO component oxides (α-quartz SiO_2 and monoclinic MO_2—as well as other silica polymorphs and the tetragonal and cubic MO_2 phases), we confirm structures and energetics agreeing to $<2\%$ with other theoretical[27–31] and experimental[32] work—well within the accuracy expected from DFT.

We quantify the thermal stability of a given MSO by its mixing energy relative to component oxides in their most stable forms:

$$\Delta E_{\mathrm{mix}} = E[M_xSi_{1-x}O_2] - xE[MO_2] - (1-x)E[SiO_2], \quad (1)$$

ΔE_{mix} is therefore expressed in units of eV/RO_2, where $R=M_xSi_{1-x}$ and $M=$Hf/Zr.

B. Structure generation

Starting geometries for hafnon and zircon have been taken as the $I4_1$ crystal structure of zircon,[25,32] and assumed transferable to hafnon due to the very similar properties of Hf and Zr compounds.[33] This 24-atom starting structure was then optimized using DFT following the computational procedure described above. Results were in overall agreement with experimental findings,[32] and, in particular, agree with the known thermodynamic stability of hafnon and zircon with respect to their component oxides. However, our calculations reveal that the stabilization energy is low: $\Delta E_{\mathrm{mix}}(ZrSiO_4)=-0.08$ eV/RO_2 and $\Delta E_{\mathrm{mix}}(HfSiO_4)=-0.06$ eV/RO_2.

The structure for zircon (hafnon) is shown in Figs. 1 and 2. It is composed of MO_8 dodecahedra with metal-oxygen distances between 2.1 and 2.3 Å, and of SiO_4 tetrahedra (abbreviated ST) with silicon-oxygen bond lengths of 1.6 Å. ST are edge linked to M dodecahedra by three-coordinate oxygen (in fact, within the structure all O atoms are three-coordinate), and alternate in $M-O_2-Si$ chains along the [0 0 1] direction, so that metal-silicon distances are 3.0 Å. The [0 0 1] chains are interconnected via $M-O_2-M$ linkages in the [1 0 0] and [0 1 0] directions. For this composition

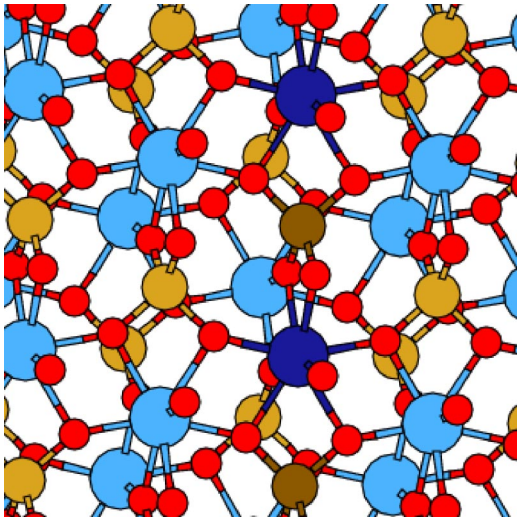


FIG. 1. Hafnon ($HfSiO_4$) or zircon ($ZrSiO_4$). A 2×2 expansion of the unit cell viewed along the [1 0 0] direction depicted by the ball-and-stick model. In order of increasing size: for black and white graphs, O (light), Si (dark), and Zr/Hf (white); and for color graphs, O (red), Si (gold), and Zr/Hf (blue). One $M-O_2-Si$ chain oriented along $z=[0\ 0\ 1]$ is highlighted (darker). See also Fig. 2.

there is a high degree of symmetry and both $M-M$ and Si–Si distances are 3.6 Å. The ST are perfectly mixed in the sense that no ST borders another.

Hafnon and zircon are the best characterized MSOs, and so their crystalline configurations are chosen to generate our starting geometries for other homogeneously mixed MSOs. A similar strategy is followed in Ref. 21. These MSOs are fully stoichiometric, with only Si–O and $M-O$ linkages (no direct $M-Si$) and all O connected to both M and Si, matching the Rutherford backscattering spectroscopy (RBS) results for as-deposited films.[14]. Appropriate substitutions are made at Hf/Zr or Si sites in the 24-atom tetragonal hafnon/zircon cell to give cells ranging in composition from M_8O_{16} to Si_8O_{16}. We thus obtain 14 symmetry-distinct compositions for each of HSO and ZSO. These unrelaxed structures with all atoms (including substituted atoms) on the initial hafnon (zircon) lattice sites are referred to as the "initial" configuration for a given composition.

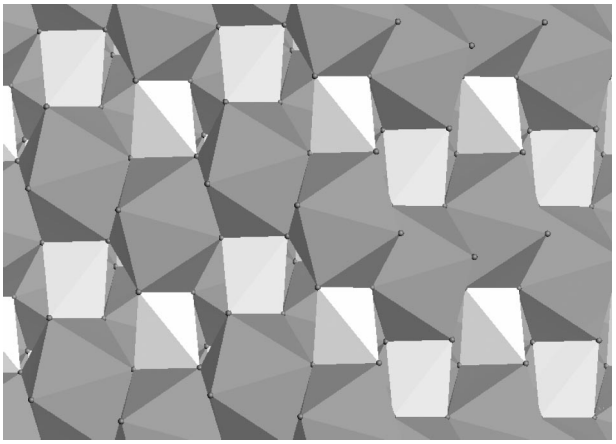


FIG. 2. Polyhedral structure of zircon/hafnon viewed along the [1 1 0] direction with SiO_4 tetrahedra displayed in light gray and MO_8 dodecahedra in dark gray. As in Fig. 1, ST and M dodecahedra are edge linked in $M-O_2-Si$ chains along $z=[0\ 0\ 1]$. There are no ST-ST linkages.

TABLE I. ZSO mixing energies ΔE_{mix} (eV/RO_2) and densities ρ (RO_2/nm^3), R=Hf/Zr,Si; see Fig. 3.

x	Cell	ΔE_{mix}^{init}	ΔE_{mix}^{pre}	ΔE_{mix}^{post}	ρ^{pre}	ρ^{post}
0.0	α-SiO_2	⋯	⋯	⋯	38.9	38.9
0.125	$Zr_1Si_7O_{16}$	+2.25	+1.37	+1.33	35.1	35.2
0.25	$Zr_2Si_6O_{16}$	+1.47	+0.98	+0.77	33.3	31.2
0.375	$Zr_3Si_5O_{16}$	+0.70	+0.62	+0.50	31.7	30.6
0.5	$Zr_4Si_4O_{16}$	−0.08	−0.08	−0.08	30.3	30.2
0.625	$Zr_5Si_3O_{16}$	+1.43	+0.25	+0.25	28.5	28.5
0.75	$Zr_6Si_2O_{16}$	+2.95	+0.51	+0.36	27.0	28.3
0.875	$Zr_7Si_1O_{16}$	+4.46	+0.75	+0.44	25.7	26.8
1.0	m-ZrO_2	⋯	⋯	⋯	35.7	35.7

For all initial configurations (substituted structures without structural relaxation), our single-point DFT calculations (Tables I and II) show that there is an energy increase of ~0.7 eV for each metal ion substituted by a silicon atom, and an energy increase of ~1.5 eV for each silicon site substituted by a M=Hf/Zr ion; substitution of a M ion onto a Si site is roughly twice as unstable than substitution of Si onto a M ion site. It is of course unphysical to assume the same coordination after these two types of substitution, and our results (Sec. III) show that improvements in coordination number drive the decomposition process. Simply relaxing the geometry may not achieve this;[20] instead, the simulation must be designed to allow substituted atoms to escape local minima and attain more appropriate coordination levels.[21]

Due to the computational restrictions, most calculations have been performed using 24-atom cells. However, for the purpose of validation a 192-atom cell has also been computed, derived from a $2\times2\times2$ expansion of the 24-atom hafnon cell. A radius relative to the center of the simulation cell was defined, and all Hf atoms lying outside this radius were substituted by Si atoms. This resulted in hafnon clusters embedded in a silica matrix, with cell composition $Hf_{13}Si_{51}O_{128}$, $x=0.20$.

C. Structure optimization and simulated annealing

After varying material composition by substitution of atoms into reference cells, atomic positions and lattice parameters are allowed to relax while minimizing the total DFT electronic energy, resulting in a local energy minimum geometry at $T=0$. These configurations resulting directly from

TABLE II. HSO mixing energies ΔE_{mix} (eV/RO_2 and densities ρ (RO_2/nm^3); see Fig. 4.

x	Cell	ΔE_{mix}^{init}	ΔE_{mix}^{pre}	ΔE_{mix}^{post}	ρ^{pre}	ρ^{post}
0.0	α-SiO_2	⋯	⋯	⋯	38.9	38.9
0.125	$Hf_1Si_7O_{16}$	+2.17	+1.34	+1.34	35.5	36.0
0.25	$Hf_2Si_6O_{16}$	+1.43	+0.95	+0.94	33.5	33.4
0.375	$Hf_3Si_5O_{16}$	+0.68	+0.55	+0.51	32.1	31.8
0.5	$Hf_4Si_4O_{16}$	−0.06	−0.06	−0.06	30.7	31.1
0.625	$Hf_5Si_3O_{16}$	+1.24	+0.26	+0.26	29.3	29.4
0.75	$Hf_6Si_2O_{16}$	+2.54	+0.52	+0.18	27.9	29.1
0.875	$Hf_7Si_1O_{16}$	+3.84	+0.77	+0.36	26.7	27.4
1.0	m-HfO_2	⋯	⋯	⋯	34.4	34.4

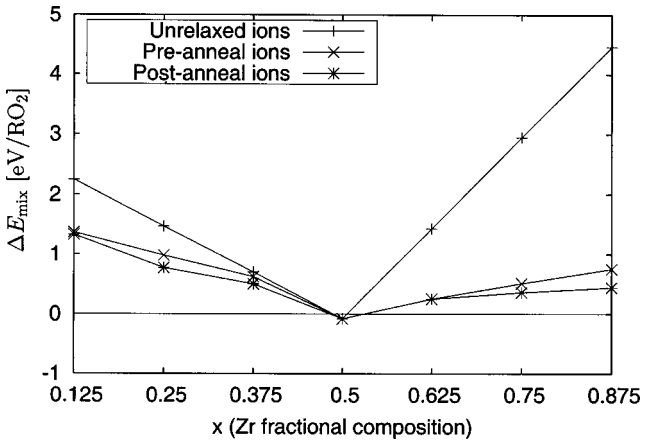


FIG. 3. ZSO mixing energies for initial, pre-, and postanneal structures. See Table I.

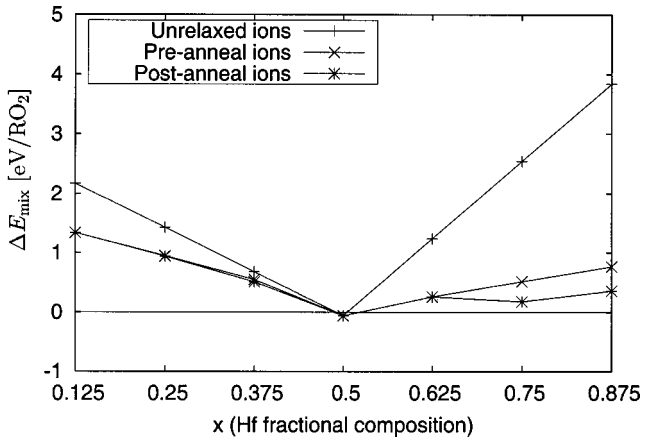


FIG. 4. HSO mixing energies for initial, pre-, and postanneal structures. See Table II.

minimization of the initial configurations are referred to as "preanneal" structures. The preanneal structures are then used as starting geometries for *ab initio* MD simulations (classical ion dynamics on the Born–Oppenheimer DFT energy surface) using VASP. The MD simulations enable local energy barriers of the order of the ionic kinetic energies to be overcome, and the ions are allowed to explore larger regions of configuration space. A time step of 1 fs was chosen. After equilibration for 1.8 ps to $T=600$ °C, Maxwell–Boltzmann-distributed random velocities are assigned (again at 600 °C) and the system is simulated for an additional 1.0 ps within the microcanonical ensemble. Instantaneous temperature fluctuations remain well below the hafnon/zircon melting points [~1700 °C (Refs. 8 and 9)]. Following the MD simulation, a final energy optimization (quench) is performed. These final structures are referred to as "postanneal" structures. If the original starting configuration is thermally stable, the final geometry from this procedure will be identical to the preanneal geometry. If the ionic kinetic energy is sufficient to overcome local energy barriers, the structures can relax to a lower-energy structure. The computational expense of our simulations requires us to consider small, periodic cells, limiting the study of large-scale effects such as amorphicity or diffusion. However, our simulation cells may be viewed as snapshots of early-stage decomposition, or as idealized representations of an evolving MO_2/SiO_2 interface.

III. RESULTS

All pre- and postanneal MSOs with compositions differing from hafnon and zircon $x \neq 0.5$ are found to be thermodynamically unstable relative to dissociation into MO_2 and SiO_2, $\Delta E_{mix} > 0$ in Eq. (1). For the ZSOs, the data are in agreement with the features of the phase diagram,[9] and it can be inferred that details of the HSO phase diagram are similar.[8] The data for the lowest-energy configurations are given in Tables I and II and depicted in Figs. 3 and 4. The approximately linear variation of energy with x matches the computed data on $x < 0.5$ ZSOs.[20]

A. Preanneal structures

On allowing the initial configurations to relax to the preanneal MSOs, there is a marked lowering in energy; see Figs. 3 and 4. As can be anticipated from the coordination numbers resulting from substitutions relative to the hafnon/zircon structures, these highly mixed structures are extremely unstable. The stabilization is larger for the MO_2-rich silicates $x > 0.5$ than for the SiO_2-rich structures $x < 0.5$. They relax to a local minimum that reduces the coordination for Si atoms, and increases that of M atoms. Despite this relaxation, the preanneal MSO's $x \neq 0.5$ remain thermodynamically unstable ($\Delta E_{mix} > 0$) and so represent local energy minima.

Figure 5 shows the atomic arrangement of $Hf_2Si_6O_{16}$ ($x=0.25$). Comparing (a) the initial configuration and (b) the preanneal structure shows that Si ions substituted into Hf sites become displaced along [0 0 1], lowering coordination to sixfold, accompanied by a shortening of Si–O distances to 1.7 Å. The original (nonsubstituted) silicon sites remain tetrahedral (Si–O=1.6 Å), but form complex polyhedra with the SiO_6 that arise from substitutions to the lattice. This is also visible in Fig. 6(a). The majority of the O atoms neighboring Si atoms distort spontaneously into a twofold coordination, giving overall 37% of O in two-coordination. This is accompanied by contraction of the cell, an 8–9% increase in density (see Tables I and II, where the density is expressed as the number of atoms, not mass, per unit volume). The structural changes in the SiO_2-rich regions of preanneal $Zr_2Si_6O_{16}$ are similar. In the regions of $x=0.25$ that remain hafnonlike, little change is apparent. The Hf/Zr sites remain largely unperturbed, maintaining eightfold coordination, with most O atoms bonded to Hf remaining threefold coordinated. The configuration changes described for $x=0.25$ reflect similar bonding rearrangements within all computed preanneal SiO_2-rich MSOs.

Similar results are observed for larger 192-atom cells such as $Hf_{13}Si_{51}O_{128}$ ($x=0.20$). The larger cell allows the Si atoms substituted to Hf sites to further reduce their coordination. The percentage of sixfold/fivefold/fourfold coordination of Si in the cell is 8%/25%/67%, indicating that Si have reduced coordination and rearranged in the SiO_2-rich regions towards optimal four coordination. The resulting percentage

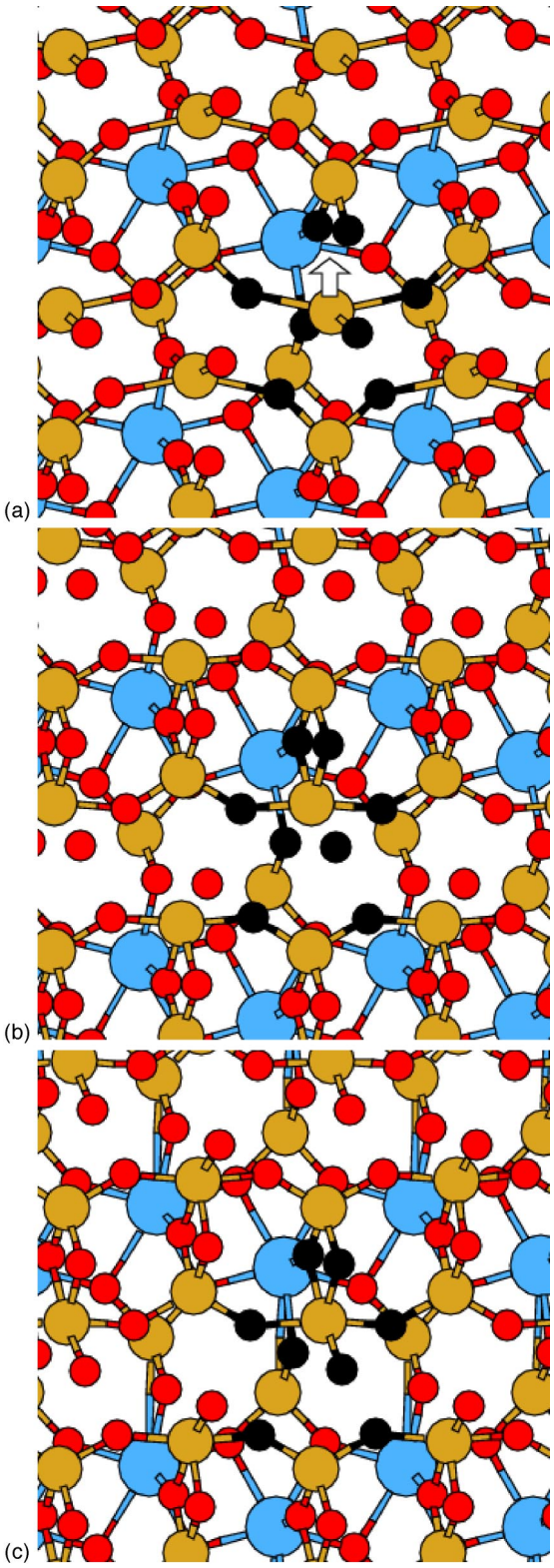


FIG. 5. A 2×2 expansion of $Hf_2Si_6O_{16}$ simulation cell viewed along [1 0 0] in ball-and-stick format. In order of increasing size: for black and white graphs, O (light), Si (dark), and Hf (white); and for color graphs, O (red), Si (gold), and Hf (blue). (a) Initial structure. Substitution of Si into half of the Hf sites of hafnon (one such site is indicated by the eight black bonded O atoms). An arrow indicates the direction of Si movement between (a) and (b). (b) Preanneal, optimized. (c) Postanneal (~600 °C), optimized. See also Fig. 6.

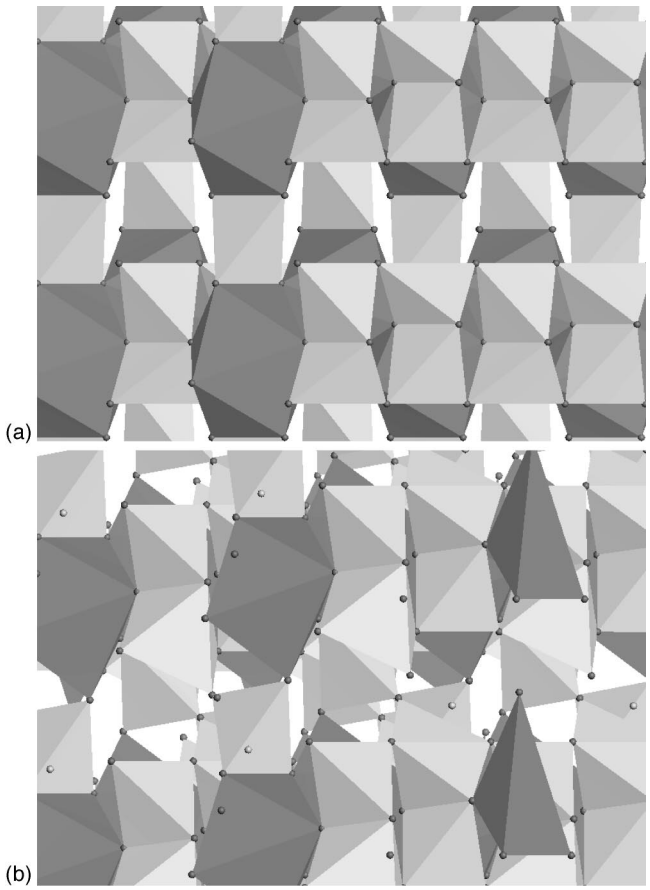


FIG. 6. Polyhedral structure of (a) preanneal $Zr_2Si_6O_{16}$ and $Hf_2Si_6O_{16}$, and (b) postanneal $Zr_2Si_6O_{16}$, viewed along [1 1 0], with silica polyhedra light gray and MO_8 dodecahedra or MO_7 decahedra dark gray. The postanneal configuration of $Hf_2Si_6O_{16}$ is similar to (a). See also Fig. 5. (a) Compared to the ideal configuration of zircon/hafnon in Fig. 2, neighboring silicon tetrahedra are formed within the SiO_2-rich regions, breaking the characteristic zircon/hafnon chains along [0 0 1]. (b) Postanneal, Zr polyhedra show distortion and a drop from eight to seven coordination, which is a motif of a monoclinic crystal structure.

of oxygen atoms in twofold/threefold coordination is 47%/53%, distributed such that in the SiO_2-rich region all O are two-coordinated and all Si are four-coordinated (except for a single three-coordinate Si). At the interface within the cell, most O bonded to Hf+Si is three-coordinate. These data indicate that the transformation to silica is complete in the SiO_2-rich regions. Of the Hf atoms, 38% have reduced their coordination to sevenfold with all other Hf atoms remaining eightfold coordinated.

For $Zr_3Si_5O_{16}$ and $Hf_3Si_5O_{16}$ ($x=0.375$), the Si atoms substituted into the lattice become fourfold coordinated with Si–O bond lengths in the range of 1.8–2.0 Å and some O atoms becoming twofold coordinated. Most of the O atoms near *M* atoms remain threefold coordinated. These bonding changes are accompanied by a small increase of 4% in density (Tables I and II).

Structural changes for $Zr_1Si_7O_{16}$ ($x=0.125$) are most significant within the SiO_2-rich regions, with Si–Si distances reduced to ~2.7 Å. Associated Si–O bonds shorten to ~1.8 Å and link to preexisting silica regions within the structure. Zr remains eightfold coordinated and O atoms near Zr tend to stay in threefold-coordinated positions. The den-

sity increases by 14% (Table I). Structural changes in $Hf_1Si_7O_{16}$ are similar with Si–Si distances ~2.7 Å, Si–O bond lengths ~1.7 Å, and a 14% increase in density (Table II).

Turning to the MO_2-rich MSOs, Fig. 7 shows $M_6Si_2O_{16}$ ($x=0.75$). In Fig. 7(a) substitution of M for Si produces fourfold-coordinated $M=$Hf/Zr within the chains along [0 0 1]. The preanneal structures [Fig. 7(b) and in polyhedral format in Fig. 8(a)] exhibit primarily displacements of M and O ions along (0 0 1), accompanied by decreases in density of 9%/11% (Hf/Zr, Tables I and II). There is still substantial strain in the structures, evidenced by the 3.1–3.8 Å range in $M-M$ distances. Unsubstituted chains are disrupted into O_2-bridged $M-$Si dimers whose local environment resembles zircon/hafnon. Displacements within the MO_2-rich chains are smaller: one M ion's local environment tends towards sixfold coordination, while other M ions remain fourfold coordinated, with two such $M=$Hf/Zr ions highlighted in Fig. 7(b). As before, the configuration changes detailed here for $x=0.75$ also describe the general trend in changes in structure and bonding for the other preanneal MO_2-rich MSOs.

For $Zr_5Si_3O_{16}$ and $Hf_5Si_3O_{16}$ ($x=0.625$), it is found that the M cation replacement for Si is largely accommodated within the structures. $M-M$ distances span the range of 3.1–3.8 Å and the cell expands to give a 5%–6% decrease in density (Tables I and II). There are no other major structural changes. For $Zr_7Si_1O_{16}$ and $Hf_7Si_1O_{16}$ ($x=0.875$) the replacement of M for Si is also largely accommodated within the structures. $M-M$ distances span 3.3–3.9 Å and the associated 13%–15% decrease in density probably reflects the longer $M-M$ distances.

B. Postanneal structures

After annealing, the SiO_2-rich structures show a further reduction in ΔE_{mix} for some ZSOs, whereas for the SiO_2-rich HSOs there is little or no change in stability between the pre- and postanneal structures. For the MO_2-rich MSOs, there is significant improvement in the relative stability for the postanneal structures with metal compositions $x>0.625$, as can be seen in Figs. 3 and 4. However, all postanneal MSOs with composition $x\neq 0.5$ remain thermodynamically unstable ($\Delta E_{mix}>0$), indicating that complete segregation into MO_2+SiO_2 is not possible for the cell sizes considered here.

Figures 5(c) and 6(b) show postanneal $Zr_2Si_6O_{16}$ ($x=0.25$) structures. Relative to preanneal, the Si atoms of the SiO_2-rich regions tend toward fivefold coordination. Remaining Zr atoms become sevenfold coordinated (not shown in the ball-and-stick view but clearly seen in the polyhedral view), Zr–Zr distances decrease to ~3.4 Å, and there is an 8° distortion in the β angle of the simulation cell: all of these results indicate a structural change toward monoclinic ZrO_2.[32] This partial crystallization/reorganization is accompanied by a 6% decrease in density. By contrast, the $Hf_2Si_6O_{16}$ structure shows no decrease in Si–Si distances on annealing [Fig. 5(c)], yielding only more ordered SiO_2-rich regions of four- and fivefold-coordinated Si, and shortened Si–O bond lengths in the range of 1.6–1.7 Å.

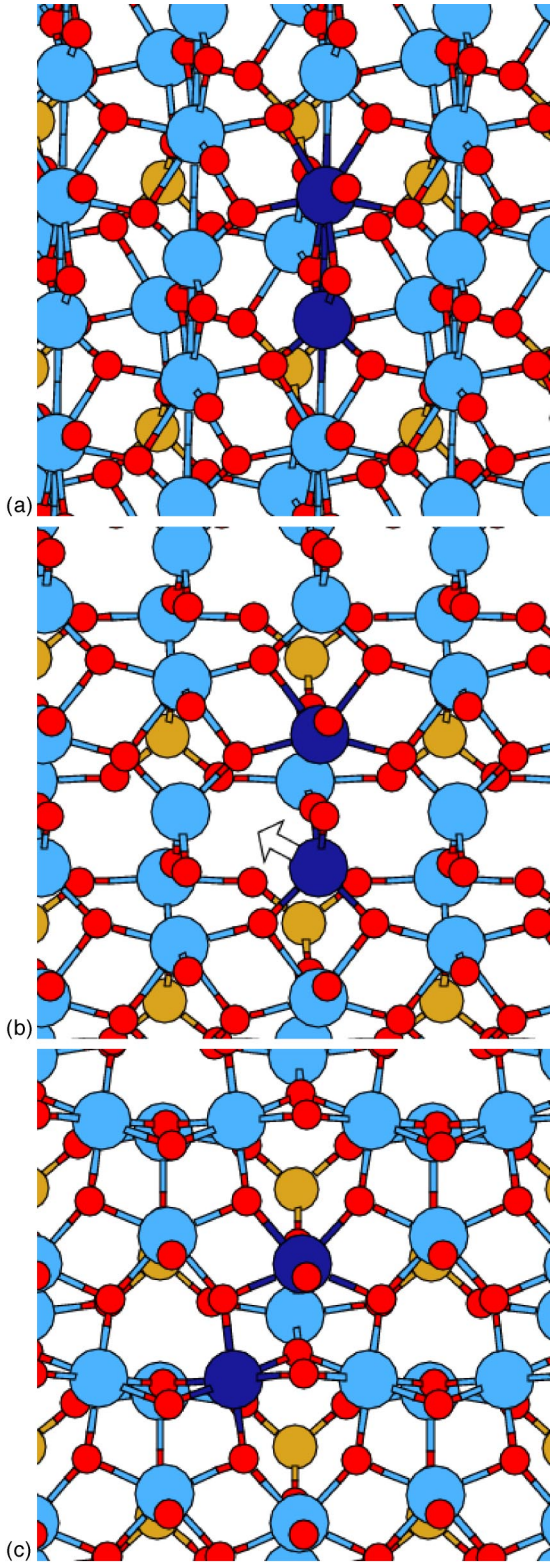


FIG. 7. A 2×2 expansion of $Hf_6Si_2O_{16}$ viewed along the [1 0 0] direction with a ball-and-stick model. In order of increasing size: for black and white graphs, O (light), Si (dark), and Hf (white); and for color graphs, O (red), Si (gold), and Hf (blue). (a) Half of the tetrahedral Si of hafnon are replaced by Hf (one such site is highlighted darker along with a neighboring Hf site). (b) Preanneal, optimized. An arrow indicates the direction of Hf movement between (b) and (c). (c) Postanneal (~600 °C), optimized. See also Fig. 8.

There are similar but less extensive changes in the SiO_2-rich regions of postanneal $Zr_3Si_5O_{16}$ and $Hf_3Si_5O_{16}$ ($x=0.375$) relative to their preanneal geometries. There emerge

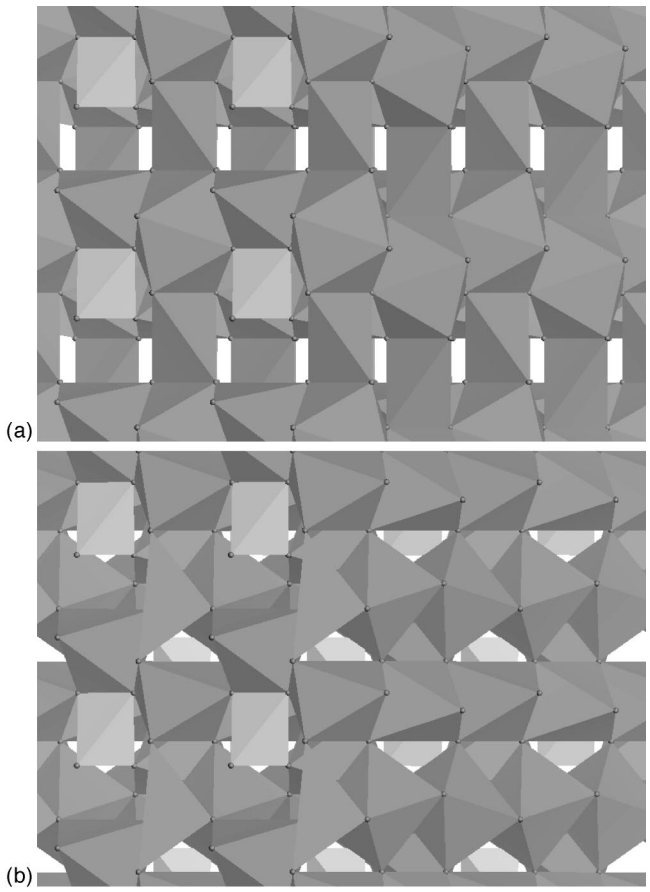


FIG. 8. Polyhedral structure of (a) preanneal $Zr_6Si_2O_{16}$ and $Hf_6Si_2O_{16}$, and (b) postanneal $Hf_6Si_2O_{16}$, viewed along [1 1 0], with SiO_4 tetrahedra (ST) light gray and metal polyhedra dark grey, with the latter comprising of MO_8 dodecahedra, MO_6 octahedra, and MO_4 tetrahedra. See also Fig. 7.

shortened Si–Si distances of 2.6 Å (in $Zr_3Si_5O_{16}$) and Si–O bonds of 1.7–1.8 Å. The density is reduced by 3% in $Zr_3Si_5O_{16}$. Apart from no significant change in density, postanneal $Zr_1Si_7O_{16}$ and $Hf_1Si_7O_{16}$ ($x=0.125$) show similar changes in Si–Si and Si–O distances. The cell angle β for the SiO_2-rich ZSOs distorts at 3°–8° between pre- and postanneal structures.

Figure 8(b) shows postanneal $Hf_6Si_2O_{16}$ ($x=0.75$) in a polyhedral view, and Fig. 7(c) shows a ball-and-stick view. A structural phase transition has occurred relative to the preanneal structure. The Hf–Hf chains aligned along [0 0 1] of the preanneal configuration are remnants of the initial hafnon structure. During anneal, we observe that these Hf atoms are able to move through an O_3 face into neighboring octahedral interstices. As a result, the HfO_2-rich region consists exclusively of edge-linked Hf octahedra in a ribbonlike arrangement along [1 0 0]. Hf–Hf distances are 3.3 Å within the ribbons and the ribbons are separated by alternate Hf–Hf distances of 3.3 and 3.9 Å. The shorter distances compare well with the ~3.2 Å obtained by extended x-ray-absorption fine structure (EXAFS) of an $x=0.55$ sample annealed at 900 °C.[34] Although puckered in the [0 0 1] direction, these Hf–O_2–Hf ribbons resemble those of rutile HfO_2.[32] However, the Hf–Hf distances are close to those found in monoclinic hafnia, which is energetically favored over rutile. There is an increase in density of 4% relative to preanneal, consistent with a change towards the more dense crystalline phase. Mixed regions of $Hf_6Si_2O_{16}$ largely maintain their hafnon structure.

In $Zr_6Si_2O_{16}$, the four-coordinate Zr only partially move through the O_3 face towards a neighboring interstice and this results in Zr coordinations in the range of 5–7. Although there is also an improvement in the packing of the polyhedra, the structural transition is not as advanced as in the $Hf_6Si_2O_{16}$ case, as indicated by Zr–Zr distances in the range of 3.5–4.0 Å. This suggests that further annealing would be necessary to achieve level of ordering of the sample measured by EXAFS (Zr–Zr ~ 3.2 Å).[34]

In $Zr_5Si_3O_{16}$ and $Hf_5Si_3O_{16}$ ($x=0.625$), the small number of M cation replacements for Si has been largely accommodated within the preanneal structures, and so, even postannealing, the $M-M$ oriented along [0 0 1] remain relatively short at 3.1 Å. However, other $M-M$ distances become spread over a greater range of values than those occurring in zircon/hafnon. At the other extreme, $Zr_7Si_1O_{16}$ and $Hf_7Si_1O_{16}$ ($x=0.875$) have undergone major structural transition to layers or ribbons of $M-O_2-M$, as described for postanneal $Hf_6Si_2O_{16}$. Hf–Hf distances under 4 Å span the range of distances found within monoclinic and cubic hafnia/zirconia. Densities increase 3%–4% with respect to preanneal values.

IV. DISCUSSION

A. Stability of zircon and hafnon

Figures 3 and 4 reveal that $ZrSiO_4$ and $HfSiO_4$ are thermodynamically stable with respect to dissociation into their component oxides, but we find that the magnitude of this ΔE_{mix} is small (Sec. II B). Analysis of their structures reveals that the thermal stability arises from the special symmetrical arrangement of SiO_4 tetrahedra (ST) and MO_8 dodecahedra. Chains of O_2-bridged $M-Si$ occur along the [0 0 1] direction, allowing for $M-M$ distances of ~3.6 Å, near the optimum $M-M$ distance found in cubic zirconia/hafnia. In addition, there are no Si–O–Si in any direction and this means that ST are isolated from one another by the surrounding M dodecahedra, preventing immediate silica formation. It is found that any deviation from these attributes creates regions of instability in the structures.

B. Spontaneous decomposition of SiO_2-rich MSOs

From the preanneal configurations considered in Sec. III A, we see that distortions occur spontaneously in the SiO_2-rich regions, increasing density and reducing Si–O bond lengths to 1.6 Å, typical of silica networks. In addition, a significant percentage of the O atoms undergo a change from threefold to twofold coordination, also typical of silica growth. This has been confirmed with calculations on large simulation cells. These SiO_2 networks appear to remain in an amorphous state, and extrapolating our findings for the SiO_2-rich MSOs to as-deposited bulk films, it is inferred that these effects lead to global segregation of a SiO_2 phase, without crystallization of SiO_2 ($<T_g \sim 1200$ °C). Contraction of Si–O and lowering of coordination number are both atomic processes that can proceed spontaneously without an

energy barrier and this is consistent with the observation of spinodal decomposition for SiO_2-rich MSOs.[11,12,18] The rate of segregation will be limited by diffusion and viscous flow at a given temperature.

Our model does not shed light on the composition of the phase that remains after SiO_2 segregation. $M-O_2-Si$ units persist in all of our calculations, characteristic of hafnon/zircon, but this is an artifact of the idealized starting structures of our model. It is likely that formation of such units is kinetically suppressed in amorphous films.[11] The experimental T_g at which MO_2 crystallization occurs in $x<0.5$ MSOs greatly exceed the T_g of bulk MO_2 (see Sec. I), which argues for a distinct mixed phase or for strong interfacial (or particle-size) effects.[35] In either case, it is possible that hafnon/zircon-like $M-O_2-Si$ units are responsible, but our model does not provide definitive evidence.

C. Metastability of MO_2-rich MSOs against nucleation

For MO_2-rich MSOs, the preanneal structures are able to accommodate the replacement of Si by four-coordinate M through distortions of the surrounding ions, consistent with the high dielectric constant of MO_2. This is accompanied by significant reductions in energies (Tables I and II). Undercoordinated M is a consequence of our choice of an initial structure, but we suggest that the preanneal distortions and postanneal segregation that we observe are general: metal ion coordination between five and eight is accommodated by distortions of the MO_2-rich regions and lattice expansion, so that these MSOs are strained, but metastable, ionic glasses.

Thermal treatment and subsequent quenching on most of the MO_2-rich MSOs result in a further slight lowering of the energy, but the associated structural changes are dramatic. A transition to a rutilelike phase is initiated within the MO_2-rich regions of $Hf_6Si_2O_{16}$, $Zr_7Si_1O_{16}$, and $Hf_7Si_1O_{16}$. Simulations show M passing through an O_3 face at elevated temperatures, but more generally we suggest that sufficient thermal excitation of soft M–O modes (such as that of Zr opposing O in zircon[25]) will mediate the transformation to nuclei of crystalline zirconia/hafnia. Indeed, the postanneal $M-M$ distances that we compute are similar to those of the monoclinic phases. We conclude that growth of MO_2 crystallites is strongly favored, but that an energetic barrier to the movement of M cations through the O sublattice must be overcome, which can be achieved by short anneals near $T_g(MO_2)$. This sequence of events is interpreted as MO_2 nucleation and will be followed by growth of crystallites[35] around MO_2 nuclei within the silicate, again consistent with experimental findings.[12,13]

D. Implications for materials design

Other computational work finds that slight differences between Hf and Zr impact the electronic and vibrational behaviors of the oxides/silicates, and hence affect the dielectric constant.[29,36] The overwhelming result of our simulations is that Hf and Zr silicates behave very similarly at the atomic scale. The differences in sizes are negligible, with Hf showing atomic and ionic radii that are 0.01 Å less than those of Zr.[36] However, there is now a consensus that, for use in the MOS gate stack, Hf-based dielectrics perform better than their Zr-based analogs. One reason is the consistently higher glass transition temperature of HSOs relative to ZSOs, at all compositions.[4] Our models provide insight as to why this is so. All simulated HSOs $x<1$ were denser than the corresponding ZSO at a given x, both pre- and postanneal (Tables I and II), so that the temperatures required for the diffusion of ions and growth of MO_2 crystallites will be higher in HSOs than in ZSOs. This is supported by the finding of Si–O–Hf adsorptions in the FTIR of HSOs, while the equivalent ZSOs showed reduced Si–O–Zr absorptions and a substantial increase in those associated with symmetric Si–O–Si (although some of these may be due to dehydration).[5]

Some individual events in the first-principles simulations support this explanation. We observe, for example, that SiO_2-rich ZSOs undergo additional changes on annealing at $\sim 600\ ^\circ C$ (increased density, shorter Si–O bonds), whereas the corresponding HSOs maintain Si–Si distances, ΔE_{mix}, and density relative to preanneal, presumably requiring higher temperatures for further segregation (Sec. III B). On the other hand, the motion of Hf across an O_3 face is observed in an individual simulated annealing MD run, whereas Zr approaches but does not cross the face. Clearly, these few MD runs do not represent a statistical sample.

Theory and experiment therefore agree that Hf and Zr pseudobinary silicates are unstable as amorphous mixtures at the $T\sim 1000\ ^\circ C$ MOS processing temperatures. One way forward is to increase T_g by further modifying the material composition, and our atomic-scale results suggest ways to achieve this. For $x<0.5$, Si–O–Si network formation may be prevented by forcing O into three coordination. For the higher-k MSOs of $x>0.5$, it may be possible to hinder M diffusion by hardening $M-O$ vibrational modes, although this would in turn reduce k.

V. CONCLUSIONS

The chemical and phase stabilities of amorphous high-k dielectrics are critical to their application in MOS technologies. In hafnium and zirconium silicates $(MO_2)_x(SiO_2)_{1-x}$, the dielectric constant increases with MO_2 content but the temperature limit for the amorphous phase decreases, implying a trade-off between maximum dielectric constant and material integrity. From our idealized models and first-principles DFT calculations, we have identified the atomic-scale driving forces which apply generally for early-stage decomposition of amorphous silicates.

SiO_2-rich silicates are found to be unstable and to undergo demixing consistent with spinodal decomposition into separate phases, driven by growth of amorphous silica networks through spontaneous lowering of O coordination and by reducing Si–Si and Si–O distances. On the other hand, MO_2-rich silicates ($M=Hf,Zr$) are metastable ionic glasses up to appropriate glass transition temperatures, because of energetic barriers to the motion of M through the O sublattice. On annealing, phase segregation is driven by $M-M$ distance optimization towards formation of MO_2 crystallites through nucleation and growth. The implication for future

electronics technology is that the zirconium and hafnium pseudobinary silicates in their pure form are unsuitable as alternatives to MOS gate dielectrics.

ACKNOWLEDGMENTS

This work was supported by the "Information Society Technologies" programme of the European Community through the HIKE project http://www.tyndall.ie/hike and by Science Foundation Ireland. We are grateful for fruitful discussions with S. Stemmer.

[1]H. R. Huff *et al.*, Microelectron. Eng. **69**, 152 (2003).
[2]G. D. Wilk, R. M. Wallace, and J. M. Anthony, J. Appl. Phys. **89**, 5243 (2001).
[3]A. I. Kingon, J. P. Maria, and S. K. Streiffer, Nature (London) **406**, 1032 (2000).
[4]S. V. Ushakov *et al.*, Mater. Res. Soc. Symp. Proc. **745**, N1.4 (2002).
[5]D. A. Neumayer and E. Cartier, J. Appl. Phys. **90**, 1801 (2001).
[6]J. D. MacKenzie, J. Am. Ceram. Soc. **47**, 76 (1964).
[7]A. Meldrum, S. J. Zinkle, L. A. Boatner, and R. C. Ewing, Nature (London) **395**, 56 (1998).
[8]V. N. Parfenenkov, R. G. Grebenshchikov, and N. A. Toropov, Dokl. Akad. Nauk SSSR **185**, 840 (1969).
[9]W. C. Butterman and W. R. Foster, Am. Mineral. **52**, 880 (1967).
[10]G. D. Wilk, R. M. Wallace, and J. M. Anthony, J. Appl. Phys. **87**, 484 (2000).
[11]S. Stemmer *et al.*, Jpn. J. Appl. Phys., Part 1 **42**, 3593 (2003).
[12]S. Stemmer *et al.*, Appl. Phys. Lett. **83**, 3141 (2003).
[13]Z. M. Rittersma *et al.*, J. Electrochem. Soc. **151**, C716 (2004).
[14]G. Rayner, Jr., R. Therrien, and G. Lucovsky, Mater. Res. Soc. Symp. Proc. **611**, C1.3 (2001).
[15]J. Kim and K. Yong, Electrochem. Solid-State Lett. **7**, F35 (2004).
[16]M. A. Quevedo-Lopez *et al.*, J. Appl. Phys. **97**, 043508 (2005).
[17]G. Lucovsky and G. B. Rayner, Appl. Phys. Lett. **77**, 2912 (2000).
[18]H. Kim and P. C. McIntyre, J. Appl. Phys. **92**, 5094 (2002).
[19]A. M. Alper, *Phase Diagrams: Materials, Science and Technology* (Academic, New York, 1970), Vol. 1; *Phase Diagrams: Materials, Science and Technology* (Academic, New York, 1978), Vol. 5.
[20]L. Ouyang and W. Y. Ching, J. Appl. Phys. **95**, 7918 (2004).
[21]G. M. Rignanese, F. Detraux, X. Gonze, A. Bongiorno, and A. Pasquarello, Phys. Rev. Lett. **89**, 117601 (2002).
[22]G. Kresse and J. Hafner, Phys. Rev. B **49**, 14251 (1994); G. Kresse and J. Furthmüller, *ibid.* **54**, 11169 (1996); Comput. Mater. Sci. **6**, 15 (1996).
[23]J. P. Perdew *et al.*, Phys. Rev. B **46**, 6671 (1992).
[24]D. Vanderbilt, Phys. Rev. B **41**, 007892 (1990); G. Kresse and J. Hafner, J. Phys.: Condens. Matter **6**, 8245 (1994).
[25]G. M. Rignanese, X. Gonze, and A. Pasquarello, Phys. Rev. B **63**, 104305 (2001).
[26]L. Stixrude, J. Geophys. Res. **107**, 2327 (2002).
[27]G. M. Rignanese, F. Detraux, X. Gonze, and A. Pasquarello, Phys. Rev. B **64**, 134301 (2001).
[28]X. Zhao and D. Vanderbilt, Phys. Rev. B **65**, 075105 (2002).
[29]X. Zhao and D. Vanderbilt, Phys. Rev. B **65**, 233106 (2002).
[30]G. Roma and Y. Limoge, Nucl. Instrum. Methods Phys. Res. B **202**, 120 (2003).
[31]C. Kohler, Z. Hajnal, P. Deak, T. Frauenheim, and S. Suhai, Phys. Rev. B **64**, 085333 (2001).
[32]R. W. G. Wyckoff, *Crystal Structures* (Interscience, New York, 1960), Vol. 1; *Crystal Structures* (Interscience, New York, 1965), Vol. 3.
[33]A. F. Cotton and G. Wilkinson, *Adv Inorg Chem*, 5th ed. (Interscience, New York, 1988).
[34]G. B. Rayner, Jr., D. Kang, C. L. Hinkle, J. G. Hong, and G. Lucovsky, Microelectron. Eng. **72**, 304 (2004).
[35]The lower surface energy of tetragonal hafnia/zirconia favors this phase for small-crystalline particles, while the energetically favored bulk phase is monoclinic.
[36]G. M. Rignanese, X. Gonze, G. Jun, K. Cho, and A. Pasquarello, Phys. Rev. B **69**, 184301 (2004).